J. Fluid Mech. (2013), *vol.* 728, *pp.* 376–395.
doi:10.1017/jfm.2013.255

Logarithmic scaling of turbulence in smooth- and rough-wall pipe flow

M. Hultmark[1],†, M. Vallikivi[1], S. C. C. Bailey[2] and A. J. Smits[1,3]

[1]Department of Mechanical and Aerospace Engineering, Princeton University, Princeton, NJ 08544, USA
[2]Department of Mechanical Engineering, University of Kentucky, Lexington, KY 40506, USA
[3]Monash University, Victoria 3800, Australia

(Received 12 June 2012; revised 14 May 2013; accepted 18 May 2013;
first published online 11 July 2013)

Measurements of the streamwise component of the turbulent fluctuations in fully developed smooth and rough pipe flow are presented over an unprecedented Reynolds number range. For Reynolds numbers $Re_\tau > 20\,000$, the streamwise Reynolds stress closely follows the scaling of the mean velocity profile, independent of the roughness, and over the same spatial extent. This observation extends the findings of a logarithmic law in the turbulence fluctuations as reported by Hultmark, Vallikivi & Smits (*Phys. Rev. Lett.*, vol. 108, 2012) to include rough flows. The onset of the logarithmic region is found at a location where the wall distance is equal to $\sim$100 times the Kolmogorov length scale, which then marks sufficient scale separation for inertial scaling. Furthermore, in the logarithmic region the square root of the fourth-order moment also displays logarithmic behaviour, in accordance with the observation that the underlying probability density function is close to Gaussian in this region.

Key words: shear layer turbulence, turbulent boundary layers, turbulent flows

1. Introduction

Here we are concerned with the scaling behaviour of hydraulically smooth, transitionally rough, and fully rough pipe flow at very high Reynolds numbers. That is, we report and examine measurements in pipe flow at Reynolds numbers Re_D from 81×10^3 to 6.0×10^6, where $Re_D = D\langle U\rangle/\nu$, D is the pipe diameter, $\langle U\rangle$ is the bulk velocity, and ν is the kinematic viscosity. In terms of the friction Reynolds number, Re_τ, this corresponds to $2.0 \times 10^3 \leqslant Re_\tau \leqslant 101 \times 10^3$, where $Re_\tau = Ru_\tau/\nu$, R is the pipe radius, and the friction velocity $u_\tau = \sqrt{\tau_w/\rho}$, where τ_w is the wall shear stress, and ρ is the fluid density.

1.1. *Scaling of hydraulically smooth flows*

When the flow is hydraulically smooth such that the smallest eddy scales are much larger than the roughness elements, classical scaling arguments indicate that the flow scaling can be divided into two regions, an 'inner region' and an 'outer region' (Millikan 1938; Perry & Abell 1975). In the inner region, where viscosity is important, the characteristic velocity scale is the friction velocity u_τ and the characteristic length

† Email address for correspondence: hultmark@princeton.edu

scale is the viscous length scale ν/u_τ. In the outer region, where viscosity is not important, the characteristic velocity scale remains the friction velocity u_τ (at least at a sufficiently high Reynolds number: see Zagarola & Smits 1998), but the characteristic length scale is now the shear layer thickness, which in a pipe is its radius R.

Classical scaling works very well for the mean velocity profile in fully developed smooth pipe flow, as comprehensively demonstrated by Zagarola & Smits (1998) and McKeon *et al.* (2004), among others (Marusic *et al.* 2010*c*; Smits, McKeon & Marusic 2011*a*). The near-wall region follows universal behaviour when scaled using inner scaling. In particular, McKeon *et al.* (2004) concluded that at sufficiently high Reynolds number there exists a viscous sublayer for $y^+ \leqslant 5$, where the inner-scaled velocity $U^+ = U/u_\tau$ varies linearly with y^+, a buffer region for $5 \leqslant y^+ \leqslant 50$, and a power-law-like region for $50 \leqslant y^+ \leqslant 600$ described by $U^+ = Cy^{+\gamma}$, where C and γ are Reynolds-number-independent constants. Here, $y^+ = yu_\tau/\nu$, where y is the distance from the wall. This power-law region has a clear resemblance to the mesolayer introduced for pipe flow by Wosnik, Castillo & George (2000), who argued that in this region there is insufficient scale separation between the energy and dissipation ranges for inertially dominated turbulence to exist. Beyond this power-law region, McKeon *et al.* (2004) noted that a 'true' logarithmic region appears, from approximately $y^+ = 600$ up to about $y/R = 0.12$, and then a universal wake region in outer coordinates fills out the remainder of the profile.

The upper and lower limits of the logarithmic region in pipe flow are still under discussion. As noted, Zagarola & Smits (1998) and McKeon *et al.* (2004) observed a lower bound close to $y^+ = 600$, while Hultmark *et al.* (2012) observed a lower limit closer to 800. Recently, Marusic *et al.* (2013) evaluated high Reynolds number measurements from boundary layer and pipe flow experiments, including those of Hultmark *et al.*, and argued that this lower bound is Reynolds-number-dependent and estimated the limit to be $y^+ = 3Re_\tau^{0.5}$. This conclusion can only hold at high Reynolds numbers, at least for pipe flow, since no logarithmic region was observed by McKeon *et al.* for $Re_\tau < 5000$. As to the upper limit, Zagarola & Smits (1998) suggested $0.07R$, whereas McKeon *et al.* (2004) indicated an upper bound of $0.12R$ and Marusic *et al.* (2013) used $0.15R$ for a mix of pipe and boundary layer flows.

Despite these ambiguities, it appears that classical scaling describes the behaviour of the mean velocity very well. In contrast, it is not so clear that the turbulent stresses follow a similar scaling, especially with regard to the streamwise component $\overline{u'^2}$. Within the near-wall region, for example, the distribution of $u^{2+} = \overline{u'^2}/u_\tau^2$ shows a distinct peak at $y^+ \approx 15$, the so-called 'inner peak'. However, the variation of this peak with Reynolds number is currently a topic of debate, with recent studies arriving at contradictory conclusions. In pipe flow, for instance, Ng *et al.* (2011) found that the magnitude of the inner peak increased with Reynolds number, whereas Hultmark, Bailey & Smits (2010), Vallikivi *et al.* (2011) and Hultmark *et al.* (2012) each found that its magnitude was constant with Reynolds number, although they disagreed on its precise value. For channel flows and boundary layer flows the picture seems clearer, in that there is a general consensus that the peak value increases with Reynolds number (Klewicki & Falco 1990; De Graaff & Eaton 2000; Marusic & Kunkel 2003; Hutchins & Marusic 2007; Jiménez & Hoyas 2008). It is worth noting, however, that its rate of increase has not yet been established with any certainty, where, for example Hutchins & Marusic (2007) proposed an increase in peak u^{2+} of 2.22 per decade in Re_τ, while Marusic, Mathis & Hutchins (2010*a*) suggest a possible value as low as 0.90 per decade. The question is important in that it informs our understanding

of inner/outer layer interactions. Marusic, Mathis & Hutchins (2010*b*) suggested that the increase in the near-wall peak for boundary layers occurs through a superposition and modulation coupling between the inner and outer regions of wall turbulence, and given that boundary layers, channel flows, and pipe flows have different geometrical constraints it would not be surprising to see differences in the structure and organization of the outer layer turbulence, and its interaction with the near-wall motions.

Further from the wall, some studies have reported the appearance of a second peak (the so-called 'outer peak') at high Reynolds number. For instance, Morrison *et al.* (2004) observed its appearance in pipe flows for $Re_\tau \geqslant 8560$. These measurements covered the range $1.8 \times 10^3 \leqslant Re_\tau < 101 \times 10^3$, and used hot-wires with $14.1 < \ell^+ < 385$, where $\ell^+ = \ell u_\tau/\nu$, and ℓ is the wire length (the lowest Reynolds number case at $Re_\tau = 1500$ has been excluded since it has been found to have a poor low-velocity calibration). The effects of spatial filtering in this investigation were obviously substantial at the higher Reynolds numbers, especially near the wall, and preferential filtering of near-wall data could have led to the appearance of a 'false' outer peak (Hutchins *et al.* 2009). To more precisely establish the nature of this outer layer behaviour, spatial filtering effects need to be minimized. In this respect, Hutchins *et al.* (2009) and Smits *et al.* (2011*b*) demonstrated that to avoid all spatial filtering effects close to the wall ℓ^+ must be smaller than 4. Smits *et al.* (2011*b*) further showed that the requirements on ℓ^+ can be relaxed linearly with the distance from the wall outside the inner peak, and proposed a correction for inadequately resolved data for wall-bounded flows on smooth surfaces.

1.2. *Scaling of transitionally and fully rough flows*

One of the more important concepts for the understanding of turbulent flows over rough surfaces is Townsend's hypothesis (Townsend 1976), which states that if the height of the shear layer, R, is much larger than the roughness height, k, the only effect of the roughness is to change the boundary condition by changing the wall shear stress. In all other respects, the flow far from the roughness elements is independent of the wall roughness. That is, when the mean flow and turbulent fluctuations are scaled by the friction velocity the profiles are universal, although the mean velocity profile in inner coordinates will be shifted downward by an amount that depends on the roughness.

Townsend's hypothesis has been confirmed by many authors (see for example Flack, Schultz & Shapiro 2005; Kunkel, Allen & Smits 2007; Allen *et al.* 2007), although some studies found the geometry of the roughness to be important through its effect on the turbulence, especially in the transitionally rough regime. Jiménez (2004) noted that most of these studies had large values of the relative roughness ratio k/R, and he proposed that the influence of the geometry of the roughness on the outer flow should diminish as $k/R \to 0$ since the information of the roughness reaches the outer flow after a long series of eddy interactions. He further stated that high-quality experiments are needed with simultaneous small k/R and large k^+ values, which implies very high Reynolds numbers. This was attempted by Kunkel *et al.* (2007), who investigated the validity of Townsend's hypothesis by comparing measurements taken in two pipes with different surface roughness for Reynolds numbers up to $Re_\tau = 100 \times 10^3$. One pipe was smooth ($k^+_{rms} < 0.25$), and other was rough so that $k/R = 3.9 \times 10^{-5}$ with k^+_{rms} up to 11, where k_{rms} is the root mean square roughness height (Shockling, Allen & Smits 2006). The results supported Townsend's hypothesis, but the authors noted that experimental

errors due to, for example, spatial and temporal filtering of the hot-wire signal added to the uncertainty, especially close to the wall where the two flows showed significant differences.

1.3. *Current study*

Here we present experimental results and scaling of turbulent pipe flow, and compare hydraulically smooth, transitionally rough and fully rough flows at very high Reynolds numbers with small relative roughness. To minimize the effects of spatial and temporal filtering, a new nanoscale thermal anemometry probe (NSTAP) was used to acquire the streamwise velocity component (Bailey *et al.* 2010; Vallikivi *et al.* 2011). The smooth-wall results were previewed by Hultmark *et al.* (2012), but the rough-wall results are presented here for the first time.

2. Experiments

Measurements of the streamwise component of the instantaneous velocity were obtained for $2.0 \times 10^3 \leqslant Re_\tau \leqslant 101 \times 10^3$. The experiments were conducted in the Princeton University/ONR Superpipe, described in detail by Zagarola & Smits (1998) and Langelandsvik, Kunkel & Smits (2007).

Two different test pipes with different relative roughnesses were used, one 'smooth' and one 'rough'. The smooth pipe was the same as that used by Zagarola & Smits (1998) and McKeon *et al.* (2004), and Morrison *et al.* (2004), with an average inner radius of $R = 64.68$ mm and a surface roughness of $k_{rms} = 0.15$ μm, resulting in a relative roughness of $k_{rms}/R = 2.3 \times 10^{-6}$. This pipe has been previously demonstrated to be hydraulically smooth for $Re_\tau < 217 \times 10^3$, which includes all Reynolds numbers tested in the current study. The rough pipe was the commercial steel pipe used by Langelandsvik *et al.* (2007) with an average inner radius of $R = 64.92$ mm and a surface roughness $k_{rms} = 5$ μm, giving $k_{rms}/R = 7.7 \times 10^{-5}$. Langelandsvik *et al.* demonstrated that this pipe is hydraulically smooth up to $Re_\tau \approx 13 \times 10^3$ and fully rough for $Re_\tau \geqslant 101 \times 10^3$.

For both pipes the measurement station was located $392R$ downstream from the entrance, to ensure fully developed flow. The streamwise pressure gradient in the pipe was measured with 21 pressure taps over a distance of $50R$ to obtain the friction velocity, u_τ. The flow conditions examined in this study are listed in table 1 and the estimated experimental uncertainties are listed in table 2.

In order to acquire data with adequate spatial and temporal resolution, NSTAPs were used for all velocity measurements reported here. Bailey *et al.* (2010) reported the first successful NSTAP measurements in grid turbulence, using a probe with sensing length $\ell = 60$ μm. The design and the manufacturing process of the probe has since been greatly improved by Vallikivi *et al.* (2011), who also used the newly designed probe to make measurements in a pipe flow at relatively low Reynolds numbers. An image of a representative 60 μm probe of the new design is shown in figure 1.

The NSTAP was operated using a Dantec StreamLine constant temperature anemometry system in the 1:1 bridge mode with an external resistor heating the NSTAP to a wire temperature of approximately 450 K. The frequency response, as measured by the usual square wave test, was always above 150 kHz in still air, which increased to more than 300 kHz at the highest Reynolds number. The data were low-pass filtered using an eighth-order Butterworth filter at 150 kHz and digitized using a 16-bit A/D board (NI PCI-6123) at a rate of 300 kHz. The initial distance between the wall and the wire, y_0, was determined using a depth-measuring microscope (Titan Tool

Case	Re_D	Re_τ	p_g (atm)	$\langle U \rangle$ (m s^{-1})	ν/u_τ (μm)	ℓ (μm)	ℓ^+	y_0 (μm)	y_0^+	k_{rms}^+
1	81×10^3	1985	0	9.48	33	60	1.8	14	0.4	0.00
2	146×10^3	3334	0.67	10.1	19	60	3.1	14	0.74	0.01
3	247×10^3	5412	2.40	8.40	12	60	5.0	14	1.2	0.01
4	512×10^3	10 481	5.43	9.37	6.2	60	9.7	14	2.3	0.02
5	1.1×10^6	20 250	10.8	10.5	3.2	60	18.8	14	4.4	0.05
6	2.1×10^6	37 690	22.5	10.5	1.7	60	35.0	14	8.2	0.09
7	4.0×10^6	68 160	45.6	10.4	0.95	60	63.2	14	15	0.16
8	4.0×10^6	68 371	45.9	10.3	0.95	30	31.7	35	37	0.16
9	6.0×10^6	98 190	69.7	10.6	0.66	30	45.5	28	43	0.23
10	993×10^3	19 316	6.88	14.8	3.4	60	17.9	28	8.5	1.49
11	2.0×10^6	36 676	13.3	16.3	1.8	60	33.9	28	16	2.82
12	3.8×10^6	69 118	22.7	19.2	0.93	60	63.9	28	30	5.32
13	5.6×10^6	100 530	34.3	19.2	0.65	60	92.9	28	44	7.74

TABLE 1. Experimental conditions. Cases 1 to 9 were measured in the smooth pipe, and cases 10 to 13 were measured in the rough pipe. Here, p_g is the pipe gauge pressure, and y_0 is the measurement location nearest to the wall.

Source	Uncertainty ±
Pressure (static and total)	0.4 %
Temperature	0.1 %
Atmospheric pressure	0.2 %
Density, ρ	0.3 %
Dynamic viscosity	0.4 %
Friction velocity, smooth flow, u_τ	0.8 %
Friction velocity, rough flow, u_τ	1.6 %
Viscous length scale, ν/u_τ	0.9 %
Wall-normal position zero, y_0	5 μm
Wall-normal position accuracy, y	10 μm m^{-1}
Distance between Pitot and hot-wire	15 μm
Wall-normal distance in inner scaling, y^+	0.53 + 0.9 %
Calibration error due to calibration velocity	0.4 %
Calibration error due to curve fitting	1.8 %
Mean velocity derived from hot-wire, U	2.2 %
Mean velocity in inner scaling (smooth), U^+	2.3 %
Mean velocity in inner scaling (rough), U^+	2.7 %
Variance of velocity, $\overline{u'^2}$	3.0 %
Variance of velocity in inner scaling (smooth), u^{2+}	3.4 %
Variance of velocity in inner scaling (rough), u^{2+}	4.7 %

TABLE 2. Uncertainty estimates.

Supply, Inc.). A stepper motor traverse with an encoder resolution of 0.5 μm (SENC50 Acu-Rite Inc.) was used to position the probe.

The NSTAP was calibrated using the pressure difference between a 0.89 mm Pitot tube and two 0.4 mm static pressure taps located in the pipe wall. The pressure difference was measured using four different pressure transducers depending on the

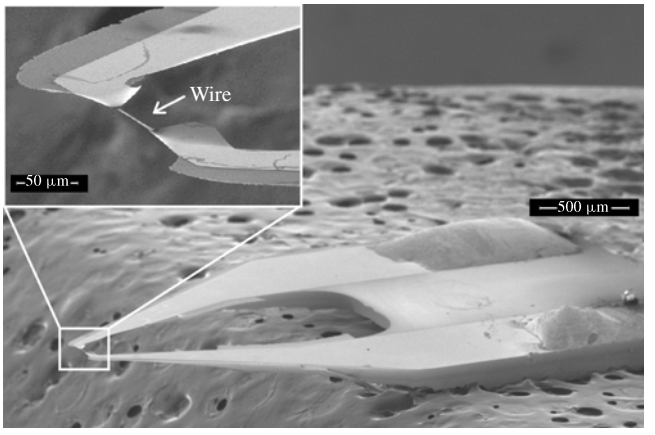

FIGURE 1. Scanning electron microscope image of a typical 60 μm NSTAP. The probe is mounted on a wax substrate for imaging (seen in background).

Reynolds number. For the lowest Reynolds number, a Datametrics 1400 transducer with a 2488 Pa range was used, and for the higher Reynolds numbers two different Validyne DP15 transducers with ranges 1379, 8618 and 34 473 Pa were employed. The Pitot tube measurements were corrected for static tap Reynolds number effects with the correlation proposed by McKeon & Smits (2002) and for viscous effects using the correlation identified by McKeon *et al.* (2003). The streamwise pressure gradient was acquired using a 133 Pa MKS Baratron transducer for the lowest Reynolds number and a 1333 Pa MKS transducer for the higher Reynolds numbers. Each pressure transducer was individually calibrated over its full range. The ambient fluid temperature change during a given profile ranged from 0.3 to 2.0 °C over the full Reynolds number range, and the data were corrected using the temperature correction outlined by Hultmark & Smits (2010). The rest of the experiment closely followed the procedures described by Hultmark *et al.* (2010).

The NSTAP manufacturing process improvements reported by Vallikivi *et al.* (2011) also allowed further reduction in the sensing length of the probe to $\ell = 30$ μm, although there is a corresponding reduction in wire aspect ratio. The analysis of Hultmark, Ashok & Smits (2011) demonstrated that end-conduction effects reduce with Reynolds number such that the sensing length of a hot-wire probe can be halved with a 15-fold increase in the Reynolds number based on sensing wire width, Re_w. No evidence of end-conduction effects were observed for the 60 μm NSTAP measurements by Bailey *et al.* (2010) at $Re_w \approx 2$, and therefore we can expect that the 30 μm NSTAP used here will continue to be free of end-conduction effects as long as $Re_w > 30$, which in the current experiments corresponds to $Re_\tau > 36 \times 10^3$. To verify the operation of the 30 μm NSTAP, we compare the streamwise Reynolds stress profile measured by this smaller probe with that measured by the 60 μm NSTAP at $Re_\tau = 68 \times 10^3$ (cases 7 and 8 in table 1), where the ℓ^+ values are 31.7 and 63.2, respectively. Figure 2 demonstrates a convincing agreement between two probes, following application of the Smits *et al.* (2011*b*) correction for spatial filtering effects. The end-conduction effects appear to be negligible for the 30 NSTAP (at least for $Re_\tau \geqslant 68 \times 10^3$), indicating that the 30 μm wire therefore is suitable for measuring at

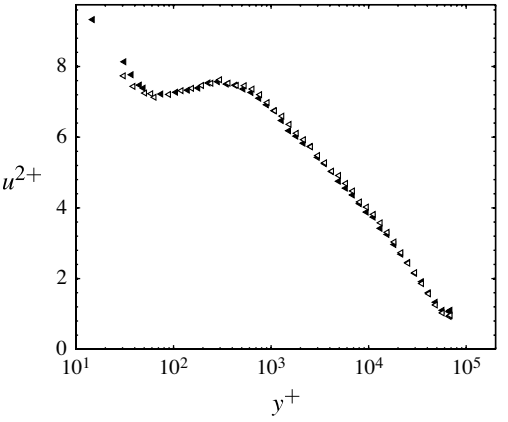

FIGURE 2. Comparison between 60 μm NSTAP (solid symbols) and 30 μm NSTAP (hollow symbols) in smooth-wall pipe flow at $Re_\tau = 68 \times 10^3$ following correction for spatial filtering effects.

these Reynolds numbers. To minimize spatial filtering effects at the higher Reynolds numbers, therefore, NSTAP probes with 30 μm sensing length were employed.

3. Results and discussion

3.1. *Mean velocity*

The mean velocity profiles for all Reynolds numbers in the smooth and rough pipes obtained using NSTAP are shown in figure 3, plotted in inner coordinates. For the smooth-wall dataset, it is clear that inner scaling collapses the data well up to the wake region whereas the rough-wall pipe, as expected, demonstrates a progressive downward shift of the profiles as k^+_{rms} increases. In all cases, the profiles display the anticipated region of logarithmic dependence given by

$$U^+ = \frac{1}{\kappa} \ln y^+ + B - \Delta U^+, \tag{3.1}$$

where ΔU^+ is the Hama roughness function (Hama 1954), and κ and B are the von Kármán and additive constants, respectively. The values $\kappa = 0.39$ and $B = 4.3$ represent a reasonable fit to the present data, and they are consistent with the values used in the recent study by Marusic *et al.* (2013). As they note, the value of $\kappa = 0.421$ obtained by McKeon *et al.* (2004) in the Superpipe using Pitot tubes exceeds the estimated uncertainty in κ of ± 0.02, but for purposes of comparison we retain the values used by Marusic *et al.* (2013). The possible reasons for differences among these estimates of κ and B are the subject of a separate study.

The Hama roughness function ΔU^+ accounts for the shift in mean velocity profiles described by Townsend (1976). Its magnitude depends on k^+_{rms} and the particular nature of the roughness. The value of ΔU^+ as a function of the equivalent sand grain roughness height, k_s, is compared in figure 4 to that found in the same pipe by Langelandsvik *et al.* (2007), who used Pitot tubes to acquire the mean velocity data. Langelandsvik *et al.* found that $k^+_s = 1.6k^+_{rms}$, which, given the good agreement shown figure 4, was also assumed for our experiments.

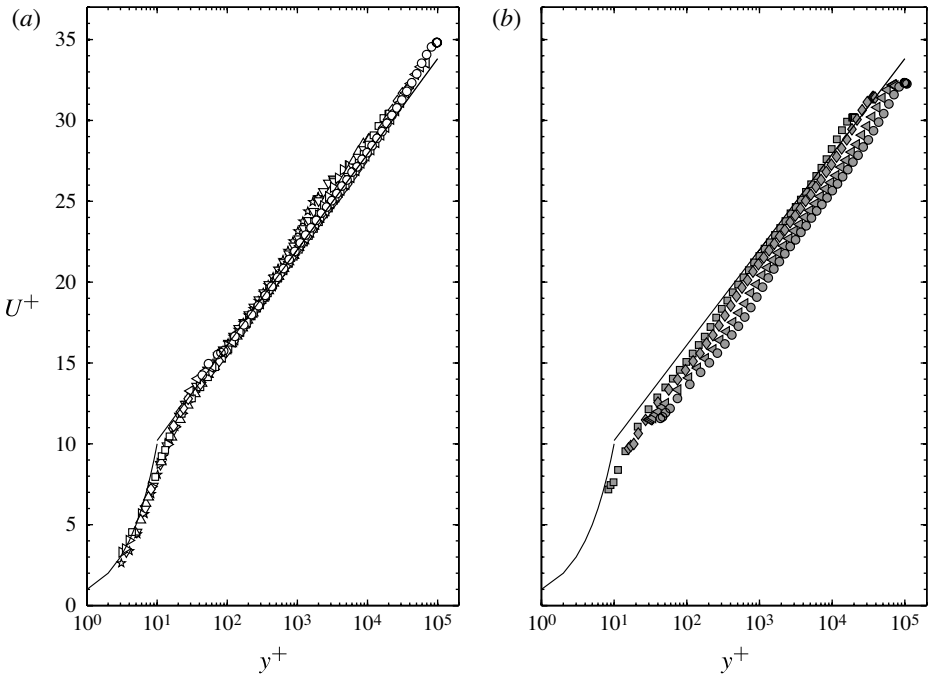

FIGURE 3. Mean velocity profiles for (*a*) smooth-wall and (*b*) rough-wall cases: ☆, $Re_\tau = 2.0 \times 10^3$; ▽, $Re_\tau = 3.3 \times 10^3$; ▷, $Re_\tau = 5.4 \times 10^3$; △, $Re_\tau = 10.5 \times 10^3$; □, $Re_\tau = 20.3 \times 10^3$; ◇, $Re_\tau = 38 \times 10^3$ (smooth), $Re_\tau = 37 \times 10^3$ (rough); ◁, $Re_\tau = 68 \times 10^3$ (smooth), $Re_\tau = 69 \times 10^3$ (rough); ◯, $Re_\tau = 98 \times 10^3$ (smooth), $Re_\tau = 100 \times 10^3$ (rough).

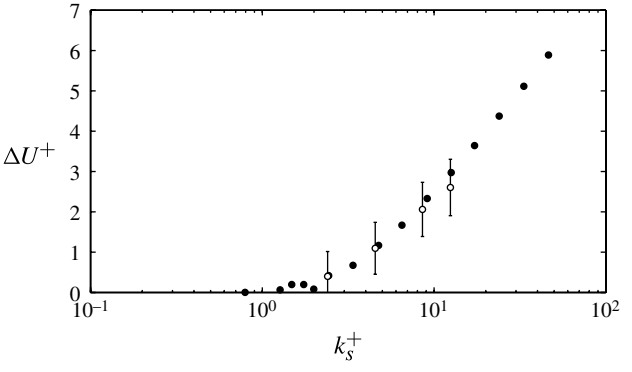

FIGURE 4. Hama roughness function as a function of non-dimensionalized roughness height $k_s^+ = 1.6k_{rms}^+$ from current study (hollow symbols) and from Langelandsvik *et al.* (2007) (solid symbols).

To better examine the range of applicability of this logarithmic scaling we define the functions

$$\Psi_1 = U^+ - \frac{1}{\kappa} \ln y^+ - B - \Delta U^+ \tag{3.2}$$

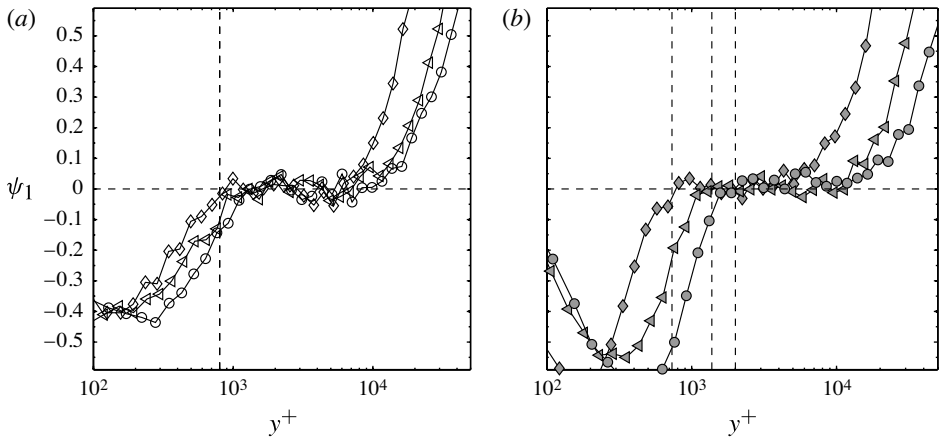

FIGURE 5. The function Ψ_1 defined by (3.2) for the three highest Reynolds numbers: (*a*) smooth pipe; (*b*) rough pipe. Symbols as in figure 3. The vertical line in (*a*) indicates $y^+ = 800$; vertical lines in (*b*) indicate $y/R = 0.02$.

and

$$\Psi_2 = U^+_{cl} - U^+ + \frac{1}{\kappa} \ln\left[\frac{y}{R}\right] \tag{3.3}$$

for the velocity profiles in inner and outer coordinates, respectively. Figure 5 shows the variation of Ψ_1 for the three highest Reynolds number cases for both smooth and rough pipes and figure 6 shows the corresponding variation of Ψ_2. To better extract the range of validity for the log law, the value of κ used to evaluate Ψ_1 and Ψ_2 for each profile was the one determined from a regression fit within the range $1000 < y^+ < 0.1Re_\tau$ for that particular profile. In all cases, the regression fit value was within the uncertainty limits of $\kappa = 0.39 \pm 0.02$.

In figure 5(*a*), the lower bound of the logarithmically scaled region appears at $y^+ \approx 800$ with the upper bound at $y/R \approx 0.15$ as illustrated in figure 6(*a*). As shown in figure 6(*b*), this upper bound describes the upper limit of the logarithmically scaled region for the rough cases as well. However, figure 5(*b*) indicates that the lower limit for the rough cases is not fixed in inner units and instead appears to be fixed at $y/k_{rms} \approx 260$ ($y/R \approx 0.02$) as shown in figure 6(*b*). Given that the upper extent of the roughness sublayer can be expected to be driven by the inertial eddies introduced by the roughness elements, it is perhaps not surprising that the lower limit scales with k_{rms} rather than ν/u_τ. The value of 260 greatly exceeds the expected extent of the roughness sublayer (2–5k_{rms}) described by Raupach, Antonia & Rajagopalan (1991), suggesting a much greater region of influence of roughness in the present case. However, considering that viscous effects for the smooth pipe are noticeable up to $y^+ = 800$, or ∼200 times the viscous sublayer thickness, it is not unreasonable that the effects of roughness extend over a similarly large distance (in terms of roughness heights) from the wall.

3.2. *Streamwise Reynolds stress*

Profiles of the streamwise Reynolds stress $u^{2+} = \overline{u'^2}/u_\tau^2$ for the smooth-wall and rough-wall pipes at all Reynolds numbers are shown in figure 7(*a*,*b*).

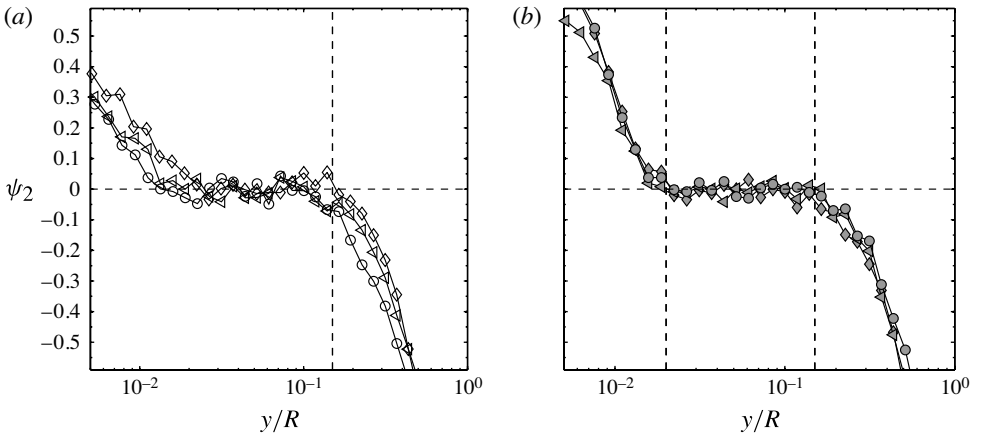

FIGURE 6. The function Ψ_2 defined by (3.3) for the three highest Reynolds numbers: (*a*) smooth pipe; (*b*) rough pipe. Symbols as in figure 3. The vertical line in (*a*) indicates $y/R = 0.15$; vertical lines in (*b*) indicate $y/R = 0.02$ and $y/R = 0.15$.

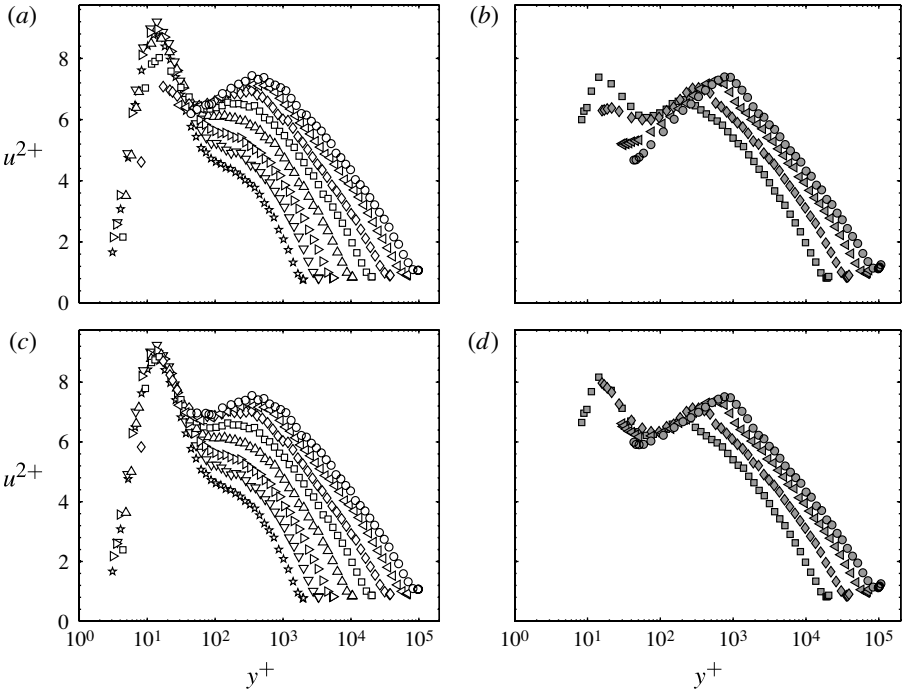

FIGURE 7. Inner-scaled streamwise Reynolds stress profiles in the (*a*) smooth pipe and (*b*) rough pipe. The same profiles corrected for spatial filtering effects following Smits *et al.* (2011*b*) are shown in (*c*) and (*d*) respectively. Symbols as in figure 3.

Consider first the effects of spatial filtering. Table 1 shows that the requirement $\ell^+ < 4$ is only met at the lowest two Reynolds numbers even with the NSTAP, and the maximum value of ℓ^+ was 46 for the smooth case and 93 for the rough case

at $Re_\tau = 10^5$. To compensate for spatial filtering effects in the smooth-wall data, the correction proposed by Smits *et al.* (2011*b*) was applied, as shown in figure 7(*c*). For the rough-wall data, the effects of spatial filtering are potentially more severe, but the correction proposed by Smits *et al.* has not been validated for measurements over rough walls. Instead, we use this correction to estimate where spatial filtering may become important. Figure 7(*d*) shows the corrected rough-wall data, but from now on we will only consider the uncorrected rough-wall data where the magnitude of the correction (if it were applied) would be less than 3 %. In general, it is apparent from figure 7 that the spatial filtering effects are mostly confined to the near-wall region ($y^+ < 200$), leaving the logarithmic and wake regions essentially unaffected.

3.3. *Inner and outer peaks in the Reynolds stress*

For the corrected smooth-wall profiles given in figure 7(*c*), it is evident that the magnitude of the inner peak is invariant with Reynolds number, within the range of 9.0 ± 0.3, agreeing with the expected u^{2+} measurement uncertainty of ± 0.3 at this location. This observation applies for $3.3 \times 10^3 < Re_\tau < 20 \times 10^3$ (for higher Reynolds numbers the inner peak was below the measurement point closest to the wall). Note that this value is somewhat higher than those previously reported in lower Reynolds number studies in this facility: 7.7 using uncorrected hot-wire probes for $691 < Re_\tau < 3336$ (Hultmark *et al.* 2010), and 8.1 using an NSTAP for $1133 < Re_\tau < 3312$ (Vallikivi *et al.* 2011). It is possible, therefore, that the uncertainty in measuring u^{2+} is concealing a slow growth of the inner peak. This problem is compounded by the temporal resolution required to fully capture the turbulence, which may help to explain the differences between the two low Reynolds number datasets because the usual frequency response of a hot-wire is considerably lower than that of a typical NSTAP.

3.4. *Logarithmic scaling in the Reynolds stress*

Logarithmic scaling of the turbulent fluctuations was first proposed by Townsend (1976), who used the attached eddy hypothesis to show that the streamwise and spanwise Reynolds stresses should follow the logarithmic variation given by

$$u^{2+} = B_1 - A_1 \ln\left[\frac{y}{R}\right] \tag{3.4}$$

within a region where the eddies scale on y, that is, within the overlap region where the mean velocity displays logarithmic scaling. Subsequently, Perry & Abell (1977) used a similarity analysis of the spectral behaviour of turbulence in smooth and rough pipe flows to suggest that, in the overlap region,

$$u^{2+} = B_1 - A_1 \ln\left[\frac{y}{R}\right] - F(y^+)^{-0.5} \tag{3.5}$$

with $B_1 = 3.53$, $A_1 = 0.8$ and $F = 6.06$. The viscous term was intended to capture the contribution of the smallest eddies to the total intensity such that (3.5) asymptotes to (3.4) at sufficiently high Reynolds number. Perry, Henbest & Chong (1986) refined the constants to suggest $B_1 = 2.67$ and $A_1 = 0.9$. These pipe flow studies were performed at relatively low Reynolds numbers ($1610 \leqslant Re_\tau \leqslant 3900$), and therefore the viscous correction term was always significant.

As first noted by Hultmark *et al.* (2012) for the smooth-wall cases, the Superpipe results provide strong support for the existence of logarithmic scaling of the streamwise turbulence component within the overlap layer. To illustrate this

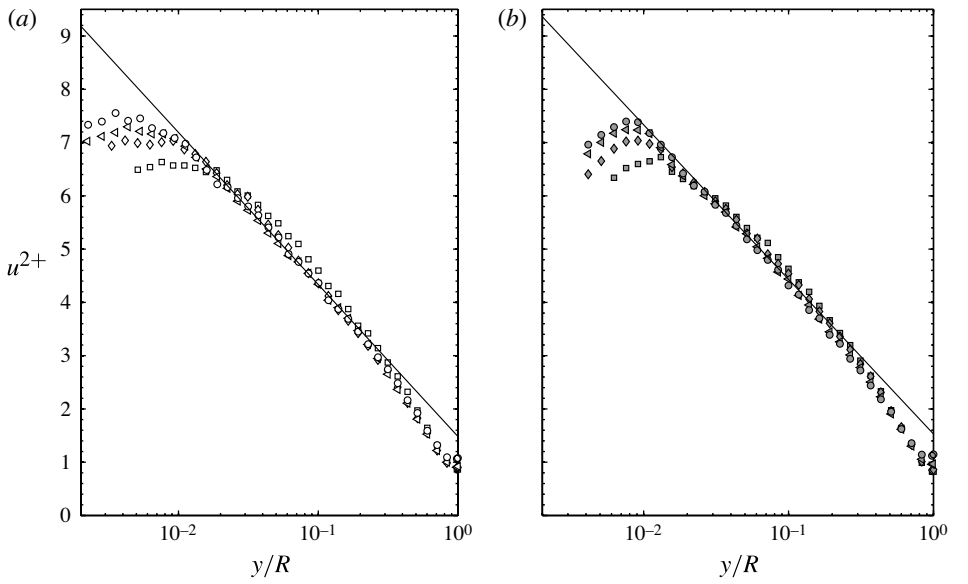

FIGURE 8. Outer-scaled streamwise Reynolds stress profiles of the four highest Reynolds numbers of (*a*) smooth-wall and (*b*) rough-wall datasets. Symbols as in figure 3, with the solid line indicating (3.4).

result, the streamwise Reynolds stress results are shown in figure 8(*a*) using outer scaling, displaying only the results for $y^+ > 100$ and for the four highest Reynolds numbers, where $F(y^+)$ is negligible. The corresponding rough-wall results are given in figure 8(*b*). The outer peak is readily apparent as a distinctive feature of both smooth and rough pipe flows, and it seems to be particularly well delineated in the rough-wall cases. However, unlike the smooth-wall cases, where the location of the outer peak appears to depend on Reynolds number (Hultmark *et al.* 2012), the outer peak for the rough-wall cases seems to be located at a fixed value of $y/k_{rms} = 100$ ($y/R = 0.008$), at least for the three highest Reynolds numbers. These figures also highlight the emergence of a logarithmic region for u^{2+} in both smooth-wall and rough-wall flows. A regression fit of the data between $y^+ = 1500$ and $y/R = 0.11$ returns $A_1 = 1.24 \pm 0.10$ and $B_1 = 1.48 \pm 0.30$ for the smooth-wall cases, and $A_1 = 1.26 \pm 0.05$ and $B_1 = 1.53 \pm 0.20$ for the rough-wall cases. Equation (3.4) with these coefficients is shown in figure 8(*a*,*b*) for comparison. Note that for a range of boundary layer flows, Marusic *et al.* (2013) gave $A_1 = 1.26$.

To better examine the range of applicability of this logarithmic scaling we define a function

$$\Psi_3 = u^{2+} + A_1 \log \frac{y}{R} - B_1. \tag{3.6}$$

Figure 9 displays Ψ_3 as a function of inner and outer scaling for the smooth-wall (figure 9*a*,*b*) and rough-wall cases (figure 9*c*,*d*). For the smooth pipe, within the scatter of the data, the streamwise Reynolds stress follows logarithmic scaling over the same region where the mean flow displays logarithmic scaling ($800 < y^+ < 0.15Re_\tau$). For the rough pipe, the upper limit for the logarithmic region appears at $y/R = 0.15$, with the lower limit scaling with k_{rms} (or R) rather than ν/u_τ, as in the case of the

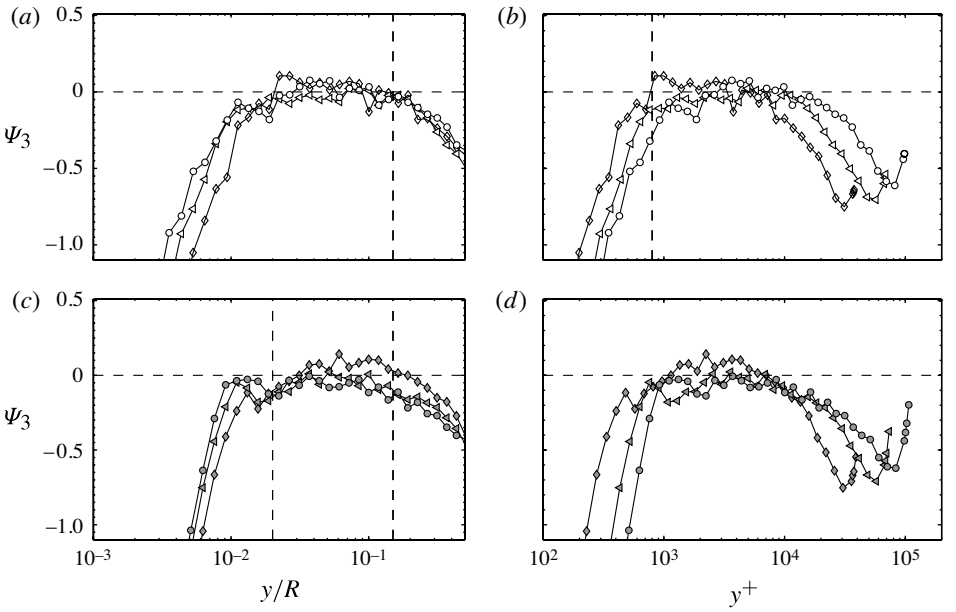

FIGURE 9. Function Ψ_3 defined by (3.6). Smooth wall: the three highest Reynolds numbers in (*a*) outer scaling, (*b*) inner scaling. Rough wall: the three highest Reynolds numbers in (*c*) outer scaling, (*d*) inner scaling. Symbols as in figure 3. The vertical dashed lines in (*a*) and (*b*) mark the location where $y/R = 0.15$, and $y^+ = 800$ respectively. In (*c*) the vertical dashed lines indicate the locations where $y/k_{rms} > 260$ and $y/R > 0.15$.

mean flow. The lower limit appears at $y/k_{rms} = 260$ ($y/R = 0.02$) with a consistent deviation below logarithmic scaling between $y/k_{rms} = 100$ and 260 for all the rough-wall cases. At sufficiently high Reynolds number, these results for the rough pipe indicate that the Reynolds stress obeys outer scaling for $y/k_{rms} > 260$, and there is an overlap between inner and outer scaling between $y/k_{rms} > 260$ and $y/R < 0.15$.

The mean velocity and the streamwise Reynolds stress distributions are shown together in figure 10, where the wall-normal locations corresponding to the upper and lower limits of the logarithmic mean velocity and Reynolds stress variation are marked by dashed lines. We see that the mean velocity and the turbulence intensity display their respective logarithmic variations over essentially the same range of wall-normal distances. This duality occurs for the smooth- and rough-wall experiments.

For the smooth-wall cases, we have seen that inner scaling in u^{2+} is observed for $y^+ < 80$, and outer scaling is observed for $y^+ > 800$. The intermediate range between these two limits approximately corresponds to that of the power-law-like region in the mean flow, suggesting that in this region the mean flow follows inner scaling, even though there is insufficient scale separation for the fluctuations to form an overlap region: dissipative scales are not fully separated from the energy-containing scales. It was found that the onset of outer scaling, that is, the lower limit of the logarithmic region, corresponds (approximately) to the location where $y/\eta \approx 100$, where η is the Kolmogorov length scale, which gives an estimate of the required scale separation. These observations are consistent with the mesolayer described by Hultmark (2012), which shows up as an offset in the logarithmic behaviour of the fluctuations. This concept is also consistent with the presence of a viscous term, as included by

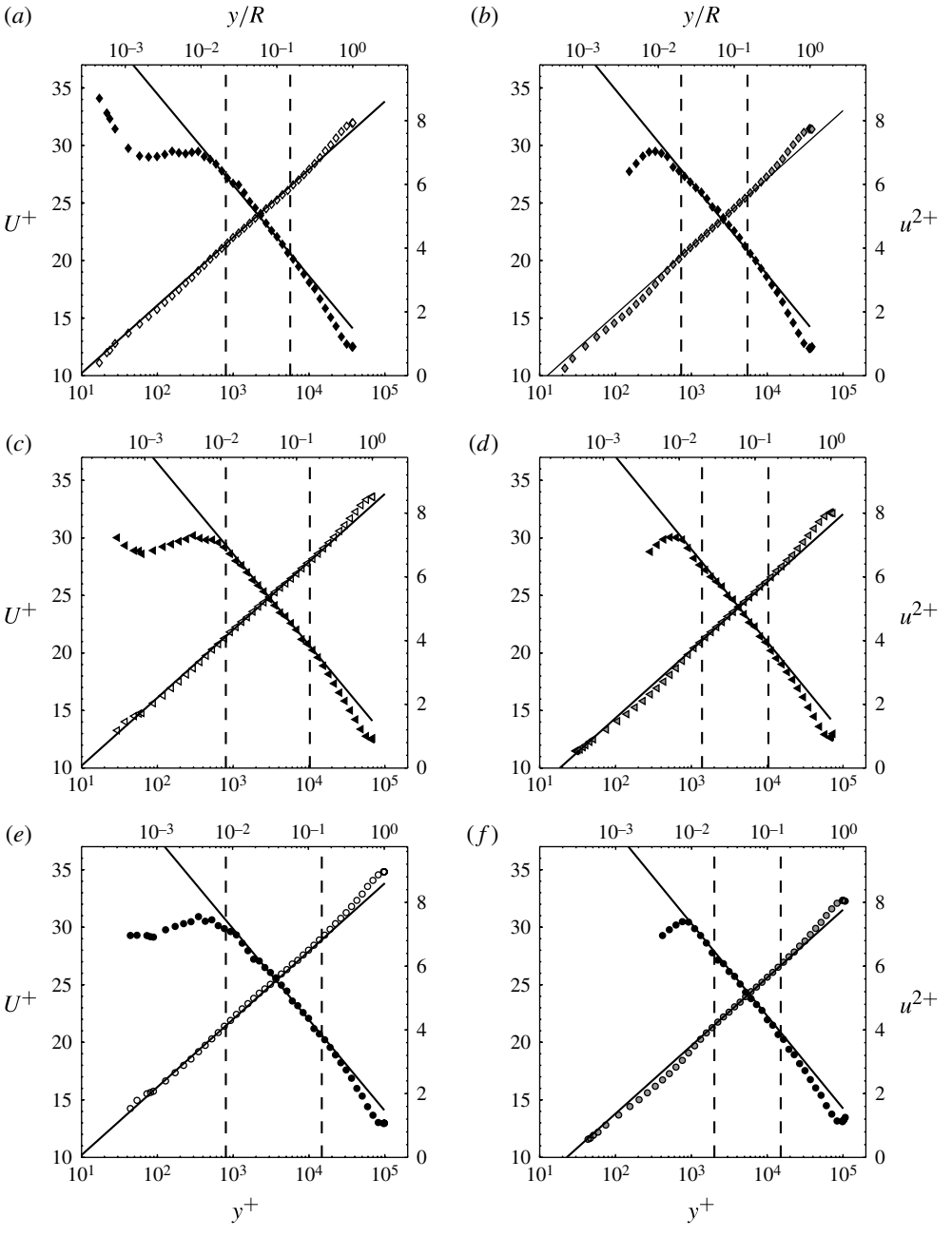

FIGURE 10. Comparison of mean (hollow symbols) and streamwise Reynolds stress (solid symbols) profiles for: (*a*) smooth-wall pipe at $Re_\tau = 38 \times 10^3$; (*b*) rough-wall pipe at $Re_\tau = 37 \times 10^3$; (*c*) smooth-wall pipe at $Re_\tau = 68 \times 10^3$; (*d*) rough-wall pipe at $Re_\tau = 69 \times 10^3$; (*e*) smooth-wall pipe at $Re_\tau = 98 \times 10^3$; (*f*) rough-wall pipe at $Re_\tau = 101 \times 10^3$. The solid lines represent (3.1) and (3.4) and dashed lines indicate their region of validity.

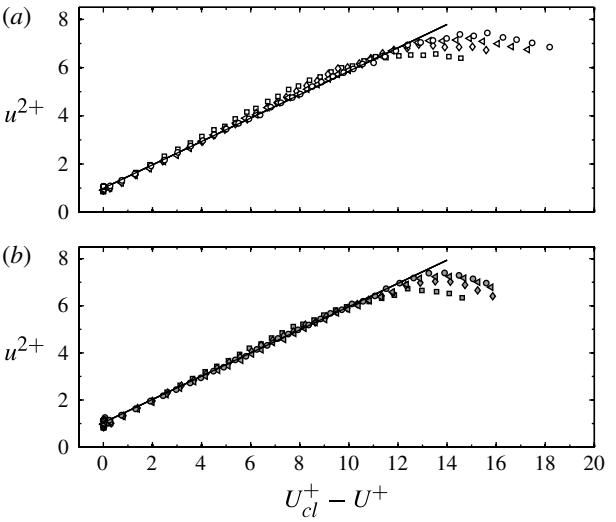

FIGURE 11. Cross-plot of streamwise Reynolds stress and mean velocity data for (*a*) smooth-wall and (*b*) rough-wall datasets, for the four highest Reynolds numbers and $y^+ > 100$. Symbols as in figure 3, with the solid line indicating (3.8).

Perry *et al.* (1986) in (3.5), since both terms act to reduce the fluctuations compared to the logarithmic equivalence closer to the wall.

3.5. *Cross-plotting logarithmic region data*

We have seen that the mean velocity and the streamwise turbulence intensity each display logarithmic behaviour over the same spatial extent. In this region, an outer-scaled log-law must also be valid for the mean velocity, where

$$U_{CL}^{+} - U^{+} = -\frac{1}{\kappa} \ln \frac{y}{R} + B^{*}, \tag{3.7}$$

where U_{CL}^{+} is the inner-scaled mean centreline velocity and B^{*} is another empirical constant, found here to be approximately 1.0. Equation (3.7) and (3.4) yield

$$u^{+2} = B_1 - A_1 \kappa B^{*} + A_1 \kappa (U_{CL}^{+} - U^{+}). \tag{3.8}$$

That is, the variance in the logarithmic region should be a linear function of the velocity defect. This representation removes the uncertainties due to ΔU^{+}, with the further advantage that any uncertainties in the wall position are eliminated because the fluctuations and the mean are measured at the same point. Figure 11, for $y^+ > 100$, shows that the data follow this linear variation, particularly for the three highest Reynolds numbers, where the viscous damping term of (3.5) is negligible. This result contradicts conventional gradient diffusion arguments, where the stresses are related to velocity gradients instead of velocity differences.

3.6. *Higher-order moments of streamwise velocity*

We now explore the behaviour of the higher-order moments, especially the third- and fourth-order central moments, $u^{3+} = \overline{u'^3}/u_\tau^3$ and $u^{4+} = \overline{u'^4}/u_\tau^4$, respectively. Morrison *et al.* (2004) found no evidence of scaling of the higher-order moments but their

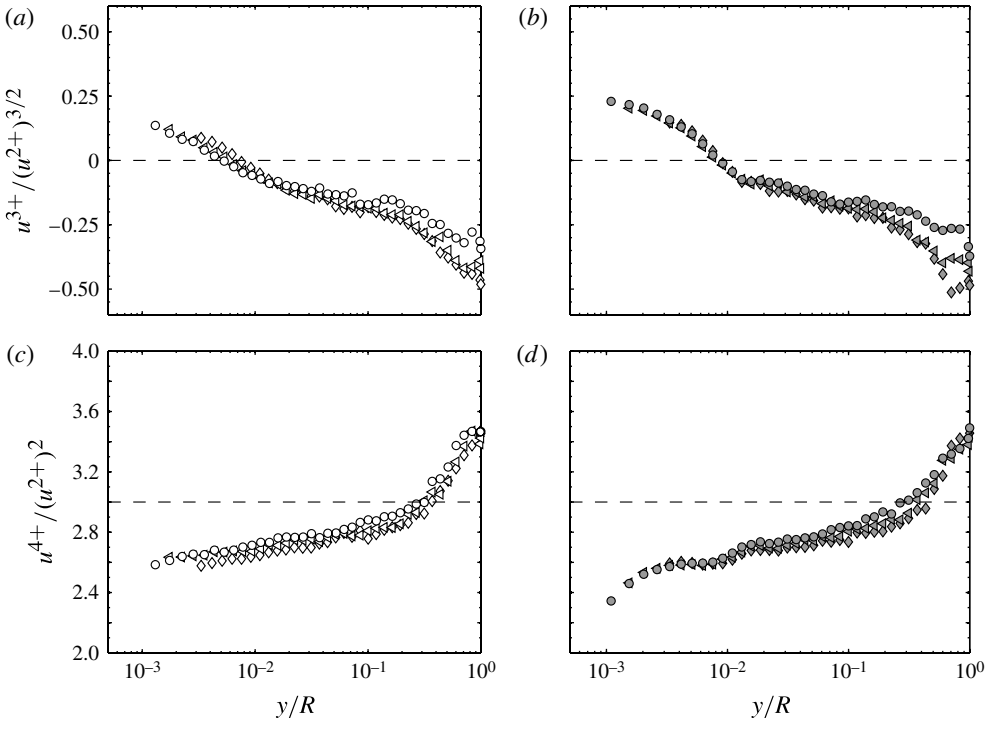

FIGURE 12. Profiles of skewness from the (*a*) smooth and (*b*) rough pipes in outer coordinates for the three highest Reynolds numbers. (*c*,*d*) Corresponding flatness profiles for smooth and rough pipes respectively. Only data points above $y^+ = 100$ are shown for clarity. Symbols as in figure 3.

results were potentially dominated by spatial filtering effects and, as observed by Bailey *et al.* (2010), spatial filtering effects become more significant with increasing order of moment. Although the NSTAP offers an improvement over conventional hot-wires, for the majority of the Reynolds numbers measured $\ell^+ > 4$, and therefore the effects of spatial resolution cannot be neglected on the higher-order moments. Hence, we limit the analysis to wall-normal locations where the spatial filtering correction of Smits *et al.* (2011*b*) predicts attenuation of u^{2+} to less than 3 %.

The skewness and flatness profiles are shown for the three highest Reynolds numbers in figure 12 for $y^+ > 100$ using outer coordinates. At these high Reynolds numbers, the results depend only weakly on Reynolds number and roughness effects. Although the flatness remains approximately constant throughout the logarithmic layer, the skewness varies over the same range of y/R, and it does not appear that the pipe flow results follow the same self-similar behaviour in the logarithmically scaled region observed in turbulent boundary layers (Tsuji, Lindgren & Johansson 2005).

As to the flatness, for a Gaussian distribution we expect it to be equal to 3, so that $u^{2+} = (u^{4+}/3)^{0.5}$. We see from figure 12 that the flatness in the logarithmic region is constant at a value of ∼2.7, so we explore the wall-normal dependence of $(u^{4+})^{0.5}$ (see also Meneveau & Marusic 2013). Figure 13 shows that there is strong support for the existence of a logarithmically scaled region in $(u^{4+})^{0.5}$ over the same Reynolds number

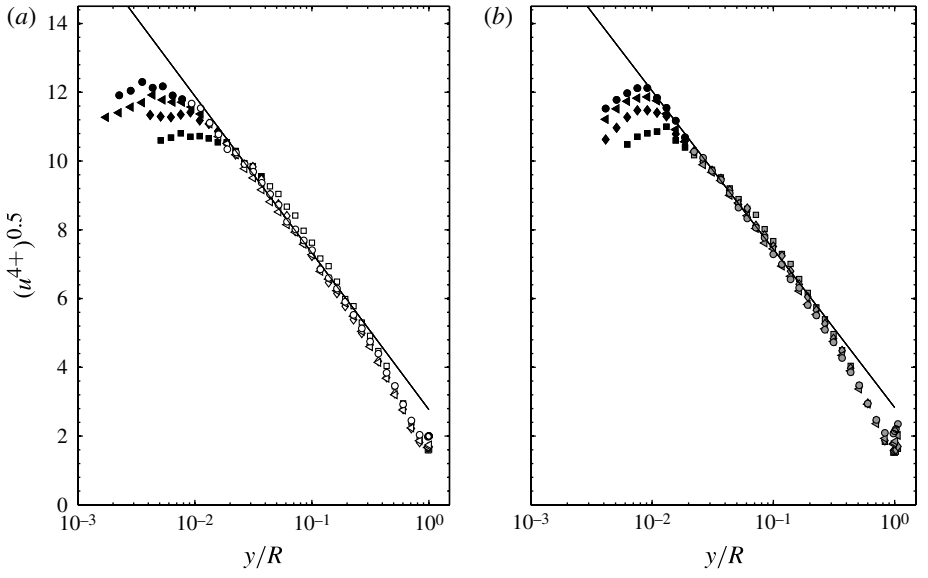

FIGURE 13. Profiles of $(u^{4+})^{0.5}$ from the (*a*) smooth and (*b*) rough pipes in outer coordinates. Symbols as in figure 3, with data points below $y^+ = 800$ for the smooth-wall flow and $y/k_{rms} = 260$ for the rough-wall flow indicated using solid symbols. For clarity, only the four highest Reynolds numbers are shown and only for $y^+ > 100$. The solid line is (3.9).

range where logarithmic scaling is evident in u^{2+}, closely following

$$(u^{4+})^{0.5} = D_1 - C_1 \log\left[\frac{y}{R}\right], \tag{3.9}$$

with $D_1 = 2.78 \pm 0.46$ and $C_1 = 1.98 \pm 0.16$ for the smooth pipe and $D_1 = 2.83 \pm 0.25$ and $C_1 = 2.00 \pm 0.06$ for the rough pipe. Note that for the smooth wall, $B_1\sqrt{3} = 2.6 \approx D_1$, and $A_1\sqrt{3} = 2.17 \approx C_1$, as expected if the probability density function followed a normal distribution (we obtain 2.73 and 2.05 if instead we use 2.7, the measured value of the flatness). Similar results are found for the rough-wall experiments.

Figure 13 also indicates that, for sufficiently high Re_τ, this logarithmic region extends over the same range of wall distance as for the mean velocity and Reynolds stress. To illustrate this point, the data points that lie below the lower logarithmic limits have been indicated in figure 13 using solid symbols. It therefore appears that the logarithmic scaling extends beyond the second moment due to the near-normality of the velocity probability density function in the log layer.

Returning to the skewness behaviour, Mathis, Hutchins & Marusic (2009) noted that there is an indication that the skewness reflects modulation of the near-wall flow by outer-scaled eddies. Similarly, the lack of scaling in the even moments within the logarithmic region at lower Reynolds numbers may indicate a significant interaction between the outer-scaled and inner-scaled eddies due to insufficient scale separation. Interestingly, once a logarithmically scaled region forms, figures 12 and 13 reveal that the location where the outer peak forms at high Re_τ closely corresponds to the location where $u^{3+} = 0$. Hence, it would appear that the outer peak is related to the modulation of the near-wall flow. We also note that, although potentially attributable

to experimental uncertainty, the weak Reynolds number dependence in u^{3+} in the outer and logarithmic layers suggests that complete similarity does not exist.

4. Conclusions

Measurements of the streamwise component of the velocity were performed in fully developed pipe flow for two pipes with different surface roughness conditions; one machined to provide a hydraulically smooth surface and the other consisting of a commercial steel pipe with irregular elements of small relative roughness. Measurements were made over a very large range of Reynolds numbers using a NSTAP to minimize contamination of the results by spatial and temporal filtering effects.

A strong duality between the scaling of the mean velocity profile and the turbulence fluctuations was observed, with an inner-scaled region extending to $y^+ \approx 50$ occupying the same span as the combination of the viscous sublayer and the buffer region in the mean velocity profile. A wake region in the turbulence intensity scales with y/R and extends outwards from $y/R > 0.15$, similar to that of the mean flow. More interestingly, logarithmic behaviour of the streamwise Reynolds stress under hydraulically smooth, transitionally rough, and fully rough conditions was observed for Reynolds numbers higher than $Re_\tau > 20 \times 10^3$, in a region corresponding to the logarithmic scaling in the mean flow. This extends the results by Hultmark *et al.* (2012) to include transitionally rough and fully rough flows. In addition, in this region of logarithmic scaling, the streamwise turbulence intensity scales with the mean velocity defect, which contradicts conventional eddy viscosity or mixing length arguments.

It was observed that the nature of the interface between the inner-scaled near-wall region and outer-scaled logarithmic region produces a peak in the streamwise Reynolds stress distribution, which appears at the same Reynolds number where the logarithmic region becomes established. This confirms earlier observations in high Reynolds number flows, where a similar outer peak has been noted. The onset of the logarithmic region is found at a location where the wall distance is equal to $\sim$100 times the Kolmogorov length scale.

Additionally, higher-order statistics were investigated and it was shown that, in the logarithmic region the square root of the fourth-order moment also displays a logarithmic region in y/R, which reflects the fact that the underlying probability density function is close to Gaussian in this region.

Acknowledgements

This work was made possible by support received through ONR grant N00014–09-1-0263, programme manager R. Joslin. H. Alfredsson of KTH suggested the cross-plotting of our data according to (3.8), and I. Marusic of the University of Melbourne suggested plotting the flatness distributions as shown in figure 13.

REFERENCES

ALLEN, J. J., SHOCKLING, M. A., KUNKEL, G. J. & SMITS, A. J. 2007 Turbulent flow in smooth and rough pipes. *Phil. Trans. R. Soc. Lond.* A **365**, 699–714.

BAILEY, S. C. C, KUNKEL, G. J., HULTMARK, M., VALLIKIVI, M., HILL, J. P., MEYER, K. A., TSAY, C., ARNOLD, C. B. & SMITS, A. J. 2010 Turbulence measurements using a nanoscale thermal anemometry probe. *J. Fluid Mech.* **663**, 160–179.

DE GRAAFF, D. B. & EATON, J. K. 2000 Reynolds-number scaling of the flat-plate turbulent boundary layer. *J. Fluid Mech.* **422**, 319–346.

FLACK, K. A., SCHULTZ, M. P. & SHAPIRO, T. A. 2005 Experimental support for Townsend's Reynolds number similarity hypothesis on rough walls. *Phys. Fluids* **17**, 035102.

HAMA, F. R. 1954 Boundary layer characteristics for smooth and rough surfaces. *Trans. Soc. Nav. Archit. Mar. Engrs* **62**, 333–358.

HULTMARK, M. 2012 A theory for the streamwise turbulent fluctuations in high Reynolds number pipe flow. *J. Fluid Mech.* **707**, 575–584.

HULTMARK, M., ASHOK, A. & SMITS, A. J. 2011 A new criterion for end conduction effects in hot wire anemometry. *Exp. Fluids* **22**, 055401.

HULTMARK, M., BAILEY, S. C. C. & SMITS, A. J. 2010 Scaling of near-wall turbulence in pipe flow. *J. Fluid Mech.* **649**, 103–113.

HULTMARK, M. & SMITS, A. J. 2010 Temperature corrections for constant temperature and constant current hot-wire anemometers. *Meas. Sci. Technol.* **21**, 105404.

HULTMARK, M., VALLIKIVI, M., BAILEY, S. C. C. & SMITS, A. J. 2012 Turbulent pipe flow at extreme Reynolds numbers. *Phys. Rev. Lett.* **108**, 094501.

HUTCHINS, N. & MARUSIC, I. 2007 Evidence of very long meandering streamwise structures in the logarithmic region of turbulent boundary layers. *J. Fluid Mech.* **579**, 1–28.

HUTCHINS, N., NICKELS, T. B., MARUSIC, I. & CHONG, M. S. 2009 Hot-wire spatial resolution issues in wall-bounded turbulence. *J. Fluid Mech.* **635**, 103–136.

JIMÉNEZ, J. 2004 Turbulent flows over rough walls. *Annu. Rev. Fluid Mech.* **36**, 173–196.

JIMÉNEZ, J. & HOYAS, S. 2008 Turbulent fluctuations above the buffer layer of wall-bounded flows. *J. Fluid Mech.* **611**, 215–236.

KLEWICKI, J. C. & FALCO, R. E. 1990 On accurately measuring statistics associated with small-scale structure in turbulent boundary layers using hot-wire probes. *J. Fluid Mech.* **219**, 119–142.

KUNKEL, G. J., ALLEN, J. J. & SMITS, A. J. 2007 Further support for Townsend's Reynolds number similarity hypothesis in high Reynolds number rough-wall pipe flow. *Phys. Fluids* **19** (5), 055109.

LANGELANDSVIK, L. I., KUNKEL, G. J. & SMITS, A. J. 2007 Flow in a commercial steel pipe. *J. Fluid Mech.* **595**, 323–339.

MARUSIC, I. & KUNKEL, G. J. 2003 Streamwise turbulence intensity formulation for flat-plate boundary layers. *Phys. Fluids* **15**, 2461–2464.

MARUSIC, I., MATHIS, R. & HUTCHINS, N. 2010*a* High Reynolds number effects in wall turbulence. *Intl J. Heat Fluid Flow* **31**, 418–428.

MARUSIC, I., MATHIS, R. & HUTCHINS, N. 2010*b* Predictive model for wall-bounded turbulent flow. *Science* **329**, 193–196.

MARUSIC, I., MCKEON, B. J., MONKEWITZ, P. A., NAGIB, H. M., SMITS, A. J. & SREENIVASAN, K. R. 2010*c* Wall-bounded turbulent flows: recent advances and key issues. *Phys. Fluids* **22**, 065103.

MARUSIC, I., MONTY, J., HULTMARK, M. & SMITS, A. J. 2013 On the logarithmic region in wall turbulence. *J. Fluid Mech.* **716**, R3.

MATHIS, R., HUTCHINS, N. & MARUSIC, I. 2009 Large-scale amplitude modulation of the small-scale structures in turbulent boundary layers. *J. Fluid Mech.* **628**, 311–337.

MCKEON, B. J., LI, J., JIANG, W., MORRISON, J. F. & SMITS, A. J. 2003 Pitot probe corrections in fully developed turbulent pipe flow. *Meas. Sci. Tech.* **14** (8), 1449–1458.

MCKEON, B. J., LI, J., JIANG, W., MORRISON, J. F. & SMITS, A. J. 2004 Further observations on the mean velocity distribution in fully developed pipe flow. *J. Fluid Mech.* **501**, 135–147.

MCKEON, B. J. & SMITS, A. J. 2002 Static pressure correction in high Reynolds number fully developed turbulent pipe flow. *Meas. Sci. Tech.* **13**, 1608–1614.

MENEVEAU, C. & MARUSIC, I. 2013 Generalized logarithmic law for high-order moments in turbulent boundary layers. *J. Fluid Mech.* **719**, R1.

MILLIKAN, C. B. 1938 A critical discussion of turbulent flows in channels and circular tubes. In *Proceedings of the Fifth International Congress of Applied Mechanics*, pp. 386–392. Wiley.

MORRISON, J. F., MCKEON, B. J., JIANG, W. & SMITS, A. J. 2004 Scaling of the streamwise velocity component in turbulent pipe flow. *J. Fluid Mech.* **508**, 99–131.

NG, H. C. H., MONTY, J. P., HUTCHINS, N., CHONG, M. S. & MARUSIC, I. 2011 Comparison of turbulent channel and pipe flows with varying Reynolds number. *Exp. Fluids* **51** (5), 1261–1281.

PERRY, A. E. & ABELL, C. J. 1975 Scaling laws for pipe-flow turbulence. *J. Fluid Mech.* **67**, 257–271.

PERRY, A. E. & ABELL, C. J. 1977 Asymptotic similarity of turbulence structures in smooth- and rough-walled pipes. *J. Fluid Mech.* **79**, 785–799.

PERRY, A. E., HENBEST, S. M. & CHONG, M. S. 1986 A theoretical and experimental study of wall turbulence. *J. Fluid Mech.* **165**, 163–199.

RAUPACH, M. R., ANTONIA, R. A. & RAJAGOPALAN, S. 1991 Rough-wall turbulent boundary layers. *Appl. Mech. Rev.* **44**, 1–25.

SHOCKLING, M. A., ALLEN, J. J. & SMITS, A. J. 2006 Roughness effects in turbulent pipe flow. *J. Fluid Mech.* **564**, 267–285.

SMITS, A. J., MCKEON, B. J. & MARUSIC, I. 2011*a* High Reynolds number wall turbulence. *Annu. Rev. Fluid Mech.* **43**, 353–375.

SMITS, A. J., MONTY, J., HULTMARK, M., BAILEY, S. C. C., HUTCHINS, M. & MARUSIC, I. 2011*b* Spatial resolution correction for turbulence measurements. *J. Fluid Mech.* **676**, 41–53.

TOWNSEND, A. A. 1976 *The Structure of Turbulent Shear Flow*. Cambridge University Press.

TSUJI, Y., LINDGREN, B. & JOHANSSON, A. V. 2005 Self-similar profile of probability density functions in zero-pressure gradient turbulent boundary layers. *Fluid Dyn. Res.* **37**, 293–316.

VALLIKIVI, M., HULTMARK, M., BAILEY, S. C. C. & SMITS, A. J. 2011 Turbulence measurements in pipe flow using a nano-scale thermal anemometry probe. *Exp. Fluids* **51**, 1521–1527.

WOSNIK, M., CASTILLO, L. & GEORGE, W. K. 2000 A theory for turbulent pipe and channel flows. *J. Fluid Mech.* **421**, 115–145.

ZAGAROLA, M. V. & SMITS, A. J. 1998 Mean-flow scaling of turbulent pipe flow. *J. Fluid Mech.* **373**, 33–79.